20th Australasian Fluid Mechanics Conference
Perth, Australia
5-8 December 2016

Stability of Flexible Inserts in Laminar Channel Flow

L. S. H. Lai[1], J. Cisonni[1] and A. D. Lucey[1]

[1]Fluid Dynamics Research Group, Department of Mechanical Engineering
Curtin University, Perth, Western Australia, 6845, Australia

Abstract

The conditions leading to the instability of a compliant insert in a laminar channel flow have been explored in numerous studies. In most, however, the analysis of this fluid–structure interaction system has focused on a limited number of cases to identify the mechanisms involved in the flow-induced oscillatory motion of the flexible structure. This study presents a parametric analysis, based on two-dimensional numerical simulations, and shows that a set of only three non-dimensional parameters can be used to provide approximations of the maximum static deflection of the flexible insert and the onset of self-excited oscillations. The investigations demonstrate that these parameters can take into account, in particular, the length of the insert and its position along the channel axial direction, and that the model remains robust for conditions leading to different instability mechanisms.

Introduction

Flow-conveying channels having compliant inserts are often associated with two major phenomena; self-excited oscillations leading to structural vibrations and disturbances in the flow, and large deformations leading to a collapse of the channel and flow limitation. In order to mitigate, control or, in some instances, take advantage of these phenomena, the fluid–structure interaction (FSI) mechanisms involved in collapsible channel flow have been extensively studied to characterise their rich diversity of static and dynamic wall deformations [5].

Detailed analyses have shown that irreversible energy transfer from the fluid to the structure leads to the onset of growing oscillations that then saturate at finite amplitude. Various modelling approaches have been used to identify the conditions driving the flow-induced instability; usually characterised by the contours of the neutral stability in a parameter space based on Reynolds number and solid-to-fluid stiffness ratio [8, 7]. However, most of these in-depth studies have only been focused on a limited number of cases. This circumscribed region of analysis within the parameter space severely limits the use of these important contributions in engineering designs or for the analysis of biomechanical systems, such as blood vessels and airways [1].

The aim of this study is to extend the scope of analysis to allow predictions of the static and dynamic motion of flexible inserts in laminar channel flow for a wide range of system geometries, solid properties and internal/external fluid flow properties. The analysis of the FSI system is carried out using numerical simulations and three non-dimensional parameters to describe the system properties.

Theoretical & Computational Modelling

The major geometric parameters of the model are shown in Fig. 1. In this FSI system, based on that of [9], fluid flow is driven by a prescribed Poiseuille velocity profile, of average velocity U^* , at the inlet of the 2-D channel of height H^* and total length L^*_{total}. The flexible insert, of length L^*_{flex}, is located on the channel upper wall at a distance L^*_{up} from the inlet. At the

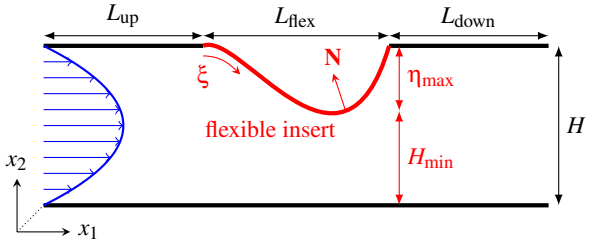

Figure 1: Schematic of the fluid–structure interaction system: 2-D channel flow with flexible insert section.

outlet, located at a distance L^*_{down} from the flexible insert, the prescribed flow is parallel and axially traction-free. The fluid has density ρ^* and dynamic viscosity μ^*. The flexible insert is massless and has thickness h^*, Young's modulus E^* and Poisson's ratio ν. It is loaded by an external pressure P^*_{ext} and the traction that the fluid exerts on it.

The open-source finite-element library `oomph-lib` [4] was used to formulate the governing equations for the viscous fluid flow and flexible insert motion. Some manipulation of these equations was performed to normalise the problem so that it is numerically better-conditioned. Variables identified with asterisks are dimensional and those without asterisks are non-dimensional. The non-dimensionalisation of the problem was done by scaling all lengths on the channel height H^*, velocities on the average inlet velocity U^*, fluid pressure on the viscous scale μ^*U^*/H^*, all solid stresses and tractions on the flexible insert's effective Young's modulus $E^*_{\text{eff}} = E^*/(1-\nu^2)$, and time on H^*/U^*.

Fluid Flow

The motion of the Newtonian fluid is governed by the non-dimensional incompressible continuity equation

$$\frac{\partial u_i}{\partial x_i} = 0 \tag{1}$$

and Navier–Stokes equations

$$Re\left(\frac{\partial u_i}{\partial t} + u_j\frac{\partial u_i}{\partial x_j}\right) = -\frac{\partial p}{\partial x_i} + \frac{\partial}{\partial x_j}\left(\frac{\partial u_i}{\partial x_j} + \frac{\partial u_j}{\partial x_i}\right) \tag{2}$$

with velocity $\mathbf{u} = u_1\mathbf{e}_1 + u_2\mathbf{e}_2$, pressure p, Cartesian coordinate $\mathbf{x} = x_1\mathbf{e}_1 + x_2\mathbf{e}_2$, time t, and Reynolds number $Re = \rho^*U^*H^*/\mu^*$. The unit vectors in the axial and transverse directions are denoted by $\mathbf{e}_1$ and $\mathbf{e}_2$, respectively. The flow is subject to the following boundary conditions:

- Poiseuille flow prescribed at the inlet ($x_1 = 0$):

$$\mathbf{u} = 6x_2(1-x_2)\mathbf{e}_1 \tag{3}$$

- parallel, axially traction-free flow at the outlet ($x_1 = L_{\text{total}}$):

$$\mathbf{u}\cdot\mathbf{e}_2 = 0 \quad \text{and} \quad \mathbf{T}\cdot\mathbf{e}_1 = 0 \tag{4a,b}$$

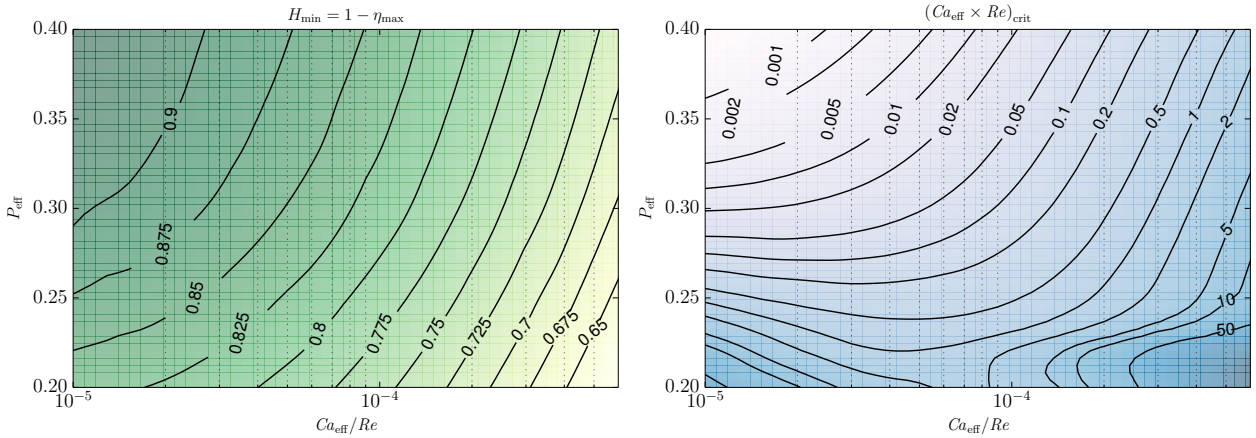

Figure 2: Contour plots of the steady-state minimum constriction of the channel $H_{\min}$ (left) and the dynamic instability threshold $(Ca_{\text{eff}} \times Re)_{\text{crit}}$ (right) as functions of the ratio Ca_{eff}/Re and the effective external pressure P_{eff}.

- no-slip on all channel walls:

$$\mathbf{u} = \mathbf{0} \quad \text{on the rigid walls} \tag{5}$$

$$\mathbf{u} = \frac{\partial \mathbf{R}}{\partial t} \quad \text{on the flexible insert} \tag{6}$$

where $\mathbf{T}$ is the fluid traction vector and $\mathbf{R}$ is the position vector to the displaced flexible insert. The fluid domain is discretised with nine-node quadrilateral Taylor–Hood elements.

Flexible Insert

The flexible insert is assumed to be infinitely thin and is modelled as an elastic beam [3, 6, 2]. It is discretised with one-dimensional, isoparametric, two-node Hermite beam elements, which are based on geometrically nonlinear Kirchhoff–Love beam theory with incrementally linear constitutive equations. The beam's undeformed shape is parametrised by a non-dimensional Lagrangian coordinate ξ and the non-dimensional position vector to a material point on the undeformed beam is given by $\mathbf{r}(\xi)$. The unit normal to the undeformed beam is denoted by $\mathbf{n}$. The applied traction $\mathbf{f} = \mathbf{f}^*/E^*_{\text{eff}}$ (a force per unit deformed length of the beam) which deforms the beam causes its material point to be displaced to the new position $\mathbf{R}(\xi)$, and the unit normal to the beam is then denoted by $\mathbf{N}$, as shown in Fig. 1. No pre-tension is applied in the flexible insert so that all the tension is induced by stretching of the insert. For the system under consideration, the non-dimensional form of the principle of virtual displacements that governs the beam deformation is given by

$$\int_0^{L_{\text{flex}}} \left(\gamma \delta\gamma + \frac{h^2}{12} \kappa \delta\kappa - \frac{1}{h} \sqrt{\frac{A}{a}} \mathbf{f} \cdot \delta\mathbf{R} \right) \sqrt{a}\, d\xi = 0 \tag{7}$$

where

$$a = \frac{\partial \mathbf{r}}{\partial \xi} \cdot \frac{\partial \mathbf{r}}{\partial \xi} \quad \text{and} \quad A = \frac{\partial \mathbf{R}}{\partial \xi} \cdot \frac{\partial \mathbf{R}}{\partial \xi} \tag{8a,b}$$

are the squares of the lengths of infinitesimal material line elements in the undeformed and deformed configurations, respectively. Therefore, the ratio $\sqrt{A/a}$ represents the stretch of the beam while the strain γ and bending κ are given by

$$\gamma = \frac{1}{2}(A - a) \quad \text{and} \quad \kappa = -(B - b) \tag{9a,b}$$

with

$$b = \mathbf{n} \cdot \frac{\partial^2 \mathbf{r}}{\partial \xi^2} \quad \text{and} \quad B = \mathbf{N} \cdot \frac{\partial^2 \mathbf{R}}{\partial \xi^2} \tag{10a,b}$$

representing the curvature of the beam, respectively, before and after the deformation.

External Pressure and Coupling

The flexible insert is loaded by an external pressure P_{ext} and the traction exerted by the fluid flowing in the channel. The non-dimensional load vector, combining these two tractions acting on its top and bottom faces, is given by

$$f_i = -P_{\text{ext}} N_i + Q \left(p N_i - \left(\frac{\partial u_i}{\partial x_j} + \frac{\partial u_j}{\partial x_i} \right) N_j \right) \tag{11}$$

where

$$Q = \frac{\mu^* U^*}{H^* E^*_{\text{eff}}} \tag{12}$$

is the ratio of the fluid pressure scale to the beam's effective Young's modulus. The non-dimensional parameter Q indicates the strength of the fluid–structure interaction.

Time-stepping was performed using a steady scheme for the flexible insert, and a BDF-2 scheme for the fluid. The FSI problem was discretised monolithically and the Newton–Raphson method was used to solve the nonlinear system of equations employing the SuperLU direct linear solver within the Newton iteration.

Results

When the compliant insert is only loaded by an external pressure, its deformation takes a regular parabolic shape, for which the maximum deflection is located at the middle of the insert. In this case, the equilibrium occurs between the external pressure and the insert tension. However, the fluid–structure interaction between the laminar channel flow and the pressure-loaded compliant insert results in deformations of more complex shapes, as qualitatively illustrated in Fig. 1, and can lead to self-excited oscillations of the flexible insert. This study focuses on predictions of two characteristics of the insert deformation, of particular interest in many engineering applications: the steady-state minimum constriction of the channel $H_{\min}$, produced by the maximum transverse deflection of the flexible insert $\eta_{\max}$, and the threshold of the self-excited insert motion. In the following, the system is described as stable if it returns to its mean state after a perturbation is applied to the mean state. It described as dynamically unstable if it amplifies the applied perturbation and

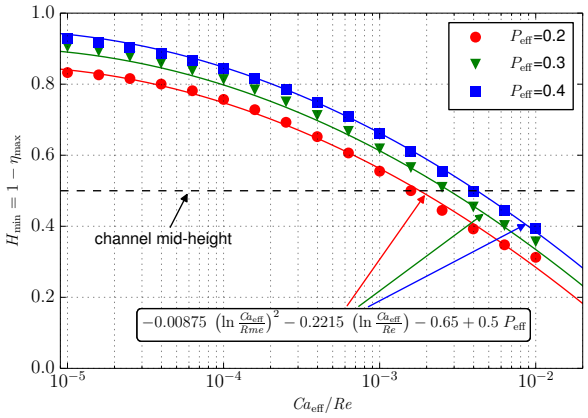

Figure 3: Steady-state minimum constriction of the channel $H_{\min}$ as a function of the ratio Ca_{eff}/Re for different effective external pressure P_{eff}.

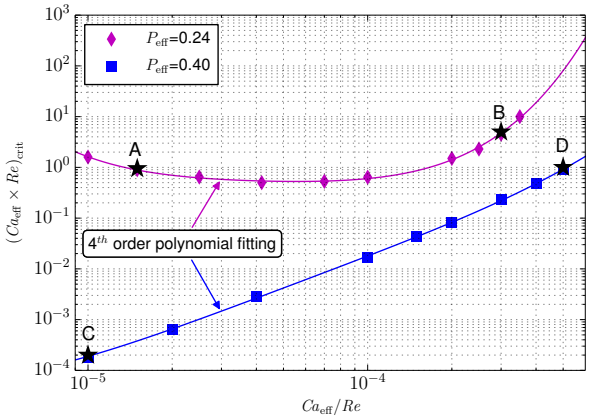

Figure 4: Dynamic instability threshold $(Ca_{\text{eff}} \times Re)_{\text{crit}}$ as a function of the ratio Ca_{eff}/Re for different effective external pressure P_{eff}.

then saturates at finite-amplitude oscillations about the mean state.

Parametric Analysis of the FSI System

A parametric study of the FSI system was used to determine the dimensional parameters that predominantly affect the flexible insert shape and the onset of self-sustaining oscillations. This leads to the characterisation of the static and dynamic behaviour of the flexible insert based on three non-dimensional parameters capturing the balance of stresses within the three components of the FSI system: flexible insert, external loading and fluid flow. The first two proposed parameters $Ca_{\text{eff}} \times Re$ and Ca_{eff}/Re are derived from characteristic non-dimensional numbers associated with the system: the Reynolds number Re and the effective Cauchy number

$$Ca_{\text{eff}} = \frac{2L^*_{\text{flex}}}{h^*} Re\, Q = \frac{2L^*_{\text{flex}}}{h^*} \frac{\rho^* U^{*2}}{E^*_{\text{eff}}} \tag{13}$$

which represents the ratio of the flow pressure coefficient acting over the length of the insert to the coefficient of tension induced in the insert due to stretching. The third proposed parameter is the effective external pressure

$$P_{\text{eff}} = \frac{2\,(P^*_{\text{ext}} - P^*_{\text{mean}})\,L^*_{\text{flex}}}{h^* E^*_{\text{eff}}} \tag{14}$$

with

$$P^*_{\text{mean}} = 12\mu^* U^* \frac{L^*_{\text{down}} + L^*_{\text{flex}}/2}{H^{*2}} \tag{15}$$

This parameter represents the ratio of net pressure loading on the insert to insert stiffness. The pressure correction term P^*_{mean} accounts for the location of the insert relative to the outlet, where the zero-pressure reference is applied.

Preliminary simulations showed that the steady-state deformation of the flexible insert is only marginally dependent on $Ca_{\text{eff}} \times Re$. However this parameter has significant impact on the dynamic instability of the system. Therefore, the steady-state minimum constriction of the channel $H_{\min}$ was determined for variations of Ca_{eff}/Re and P_{eff}. The threshold of instability was characterised by the critical value of $Ca_{\text{eff}} \times Re$, needed to observe oscillatory motion of the insert about its mean position, also for variations of these two parameters. Figure 2 shows the changes in $H_{\min}$ and $(Ca_{\text{eff}} \times Re)_{\text{crit}}$ over the $\{Ca_{\text{eff}}/Re, P_{\text{eff}}\}$ parameter space. It can be seen that the steady-state minimum constriction of the channel follows a similar trend for all the considered values of effective external pressure and decreases as the ratio Ca_{eff}/Re increases. However, the evolution of the dynamic instability threshold as a function of the ratio Ca_{eff}/Re changes depending on the value of effective external pressure. For $P_{\text{eff}} > 0.3$, the system becomes more stable (increase in $(Ca_{\text{eff}} \times Re)_{\text{crit}}$) as Ca_{eff}/Re increases. For $P_{\text{eff}} < 0.3$, the system is first destabilised with the increase in Ca_{eff}/Re but becomes more stable as Ca_{eff}/Re continues to increase.

Steady-State Minimum Constriction

The results of the FSI system analysis show that the shape of the deformed flexible insert can vary significantly depending on the values of effective external pressure and ratio Ca_{eff}/Re. Thus, the locus along the flexible insert where the transverse deflection is maximal can move in the axial direction. However, the variation of the maximum transverse deflection $\eta_{\max}$, hence of the minimum constriction $H_{\min} = 1 - \eta_{\max}$, as a function of the ratio Ca_{eff}/Re follows a regular trend, as shown in Fig. 3. The change in P_{eff} value generates a vertical translation of the $H_{\min}$ curves. Therefore, the data obtained from the numerical simulations can be fitted to yield an analytical expression of the minimum constriction in the channel:

$$\begin{aligned} H_{\min} = &-0.00875 \left(\ln \frac{Ca_{\text{eff}}}{Re}\right)^2 \\ &-0.2215 \left(\ln \frac{Ca_{\text{eff}}}{Re}\right) - 0.65 + 0.5\, P_{\text{eff}} \end{aligned} \tag{16}$$

This expression provides a reasonably good approximation of the non-dimensional minimum constriction, which indicates the severity of the obstruction produced by the flexible insert ($H_{\min} = H^*_{\min}/H^*$), for a wide range of system configurations, here described in terms of the non-dimensional parameters P_{eff} and Ca_{eff}/Re.

Self-Sustaining Oscillations

The results of the parametric study of the FSI system show that the evolution of the instability threshold as the ratio Ca_{eff}/Re increases exhibits different trends depending on the effective external pressure. As shown in Fig. 4, for a relatively high external pressure ($P_{\text{eff}} = 0.4$), the system becomes more stable to applied perturbations as the ratio Ca_{eff}/Re increases. For a lower external pressure ($P_{\text{eff}} = 0.24$), the curve of the critical product $Ca_{\text{eff}} \times Re$ has a minimum, indicating that the system becomes

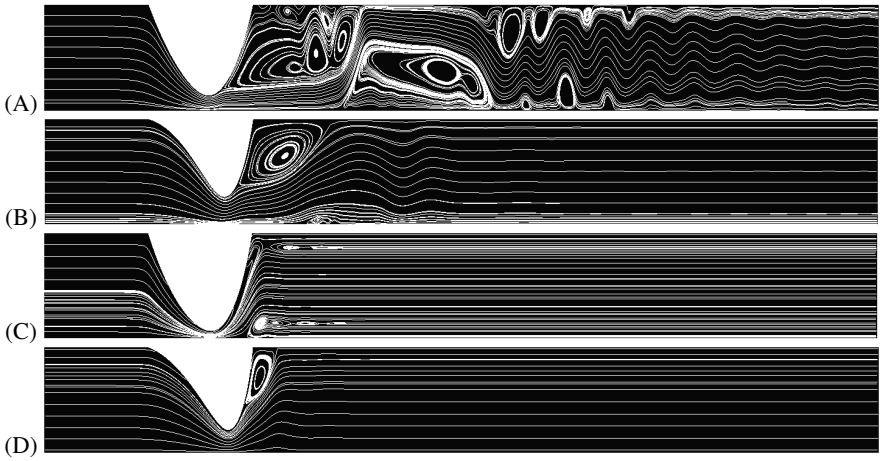

Figure 5: Instantaneous streamlines at the time step for which the oscillatory transverse deflection of the flexible insert is maximal. Cases A, B, C and D correspond to system configurations indicated in Fig. 4. Scaling of spanwise dimension is 5:1 compared to streamwise dimension.

more easily unstable over a range of Ca_{eff}/Re. This difference in trends suggests that different mechanisms are at play in the fluid–structure interaction depending on the system conditions. Thus, major changes in the flow behaviour near the constricted region of the channel can be observed when the viscous effects become more important. Figure 5 shows the streamlines in the flow for four cases for which the system conditions, as indicated in Fig. 4, lead to finite-amplitude oscillations of the flexible insert. It can be observed that for cases A, B and D, the flow detaches from the deformed flexible insert just downstream of the most constricted cross-section of the channel. A recirculation zone is therefore formed downstream of the flexible insert near the upper rigid wall. For these three cases, the difference in conditions does not have significant impact on the flow behaviour but influences the size of the recirculation zone and the amplitude of the perturbations in the flow convected downstream of the constricted region. For case C, however, the flow remains attached to the flexible insert almost over its whole length. A smaller recirculation zone is then created near the lower rigid wall. Therefore, the pressure distribution along the flexible insert is significantly different for case C in comparison to the three other cases.

Conclusions

A parametric study of a flow-conveying channel having a compliant insert subjected to an external pressure was performed to determine the parameters required for self-sustained oscillations to occur. Three non-dimensional parameters, $Ca_{\text{eff}} \times Re$, Ca_{eff}/Re and P_{eff}, were proposed to describe the system properties and allow prediction of two major characteristics of the insert deformation. The steady-state maximum deflection of the flexible insert was found to be predominantly linked to the ratio Ca_{eff}/Re and the effective external pressure P_{eff}. Data obtained from the numerical simulations were fitted to yield an analytical expression of this system characteristic. The threshold of FSI instability was found to be associated with a critical value of the product $Ca_{\text{eff}} \times Re$. Therefore, the onset of self-sustained oscillations of the insert deformation could be predicted from the three non-dimensional parameters.

Acknowledgements

The authors would like to thank the Australian Government through the Australian Postgraduate Award (APA) and Curtin University for their financial support.

References

[1] Bertram, C., Fluid flow in distensible vessels, *Clinical and Experimental Pharmacology and Physiology*, **36**, 2009, 206–216.

[2] Cisonni, J., Lucey, A.D. and Elliott, N.S.J., Stability of a cantilevered flexible plate with non-uniform thickness in viscous channel flow, *Proceedings of the 3rd Symposium on Fluid-Structure-Sound Interactions and Control*, editors Zhou, Y., Lucey, A.D., Liu, Y. and Huang, L., Springer, 2016.

[3] Elliott, N.S.J., Lucey, A.D. and Heil, M., Large-amplitude oscillations of a finite-thickness cantilevered flexible plate in viscous channel flow, *Proceedings of the 3rd Joint US-European Fluids Engineering Summer Meeting and 8th International Conference on Nanochannels, Microchannels and Minichannels*, 2010.

[4] Heil, M. and Hazel, A.L., `oomph-lib` — an Object-Oriented Multi-Physics Finite-Element Library, *Fluid-Structure Interaction*, editors Schäfer, M. and Bungartz, H.-J., Springer, 2006, 19–49.

[5] Heil, M. and Jensen, O., Flows in deformable tubes and channels theoretical models and biological applications, *Fluid Mechanics and Its Applications*, **72**, 2003, 15–50.

[6] Lai, L. Lucey, A.D., Elliott, N.S.J. and Pitman, M.D., Computational modelling of a fluid-conveying flexible channel using oomph-lib, *Proceedings of the 19th International Congress on Modelling and Simulation*, 2011, 565–571.

[7] Liu, H.F., Luo, X.Y., Cai, Z.X. and Pedley., T.J., Sensitivity of unsteady collapsible channel flows to modelling assumptions, *Communications in Numerical Methods in Engineering*, **25**, 2009, 483–504.

[8] Luo, X.Y., Cai, Z.X., Li, W.G. and Pedley, T., The cascade structure of linear instability in collapsible channel flows, *Journal of Fluid Mechanics*, **600**, 2008, 45–76.

[9] Pedley, T., Longitudinal tension variation in collapsible channels: A mechanism for the breakdown of steady flow, *ASME Journal of Biomechanical Engineering*, **114**, 1992, 60–67.